Matter and Radiation at Extremes RESEARCH ARTICLE scitation.org/journal/mre

Generation of highly-polarized high-energy brilliant γ-rays via laser-plasma interaction

Cite as: Matter Radiat. Extremes 5, 054402 (2020); doi: 10.1063/5.0007734
Submitted: 16 March 2020 • Accepted: 12 July 2020 •
Published Online: 30 July 2020

Kun Xue,[1] Zhen-Ke Dou,[1] Feng Wan,[1] Tong-Pu Yu,[2] Wei-Min Wang,[3] Jie-Ru Ren,[1] Qian Zhao,[1] Yong-Tao Zhao,[1] Zhong-Feng Xu,[1] and Jian-Xing Li[1,a)]

AFFILIATIONS

[1]MOE Key Laboratory for Nonequilibrium Synthesis and Modulation of Condensed Matter, School of Science, Xi'an Jiaotong University, Xi'an 710049, China
[2]Department of Physics, National University of Defense Technology, Changsha 410073, China
[3]Department of Physics and Beijing Key Laboratory of Opto-Electronic Functional Materials and Micro-Nano Devices, Renmin University of China, Beijing 100872, China

Note: This paper is part of the Special Issue on Progress in Matter and Radiation at Extremes in China.

[a)]**Author to whom correspondence should be addressed:** jianxing@xjtu.edu.cn

ABSTRACT

The generation of highly polarized high-energy brilliant γ-rays via laser–plasma interaction is investigated in the quantum radiation-reaction regime. We employ a quantum electrodynamics particle-in-cell code to describe spin-resolved electron dynamics semiclassically and photon emission and polarization quantum mechanically in the local constant field approximation. As an ultrastrong linearly polarized (LP) laser pulse irradiates a near-critical-density (NCD) plasma followed by an ultrathin planar aluminum target, the electrons in the NCD plasma are first accelerated by the driving laser to ultrarelativistic energies and then collide head-on with the laser pulse reflected by the aluminum target, emitting brilliant LP γ-rays via nonlinear Compton scattering with an average polarization of about 70% and energy up to hundreds of MeV. Such γ-rays can be produced with currently achievable laser facilities and will find various applications in high-energy physics and laboratory astrophysics.

I. INTRODUCTION

Polarized high-energy γ-rays have a wide range of significant applications, for example, in generating polarized positrons and electrons,[1,2] probing radiation mechanisms and properties of dark matter[3] and black holes,[4] exciting polarization-dependent photo-fission of nuclei in giant dipole resonances,[5] meson photoproduction,[6] and detecting vacuum birefringence in ultrastrong laser fields.[7–11] Such γ-rays are commonly produced through either bremsstrahlung[12,13] or linear Compton scattering.[14–16] However, the former cannot generate linearly polarized (LP) γ-rays, suffers from the deficiencies of large scattering angle and divergent emission in the incoherent regime,[17] and is limited to a low current density of the impinging electrons and a low radiation flux owing to the risk of damage to crystalline materials in the coherent regime,[18–20] while the latter is severely restricted by the low electron–photon collision luminosity due to the low laser intensities.

Nowadays, with rapid developments in high-power laser technology, state-of-the-art laser facilities can provide laser beams with peak intensities of the order of 10^{22} W/cm^2, pulse durations of tens of femtoseconds, and energy fluctuations of ~1%,[21–27] which have stimulated experimental investigations of quantum electrodynamics (QED) processes during laser–plasma or laser–electron beam interactions.[28,29] Such strong laser fields can be employed to directly polarize electrons[30–36] through radiative spin effects and to create polarized positrons[37,38] through the asymmetry in spin-resolved pair production probabilities. Moreover, in such strong laser fields, the Compton scattering process moves into the nonlinear regime: during laser–electron interaction, the electron radiates a high-energy γ-photon by absorbing millions of laser photons.[28] Highly polarized high-energy brilliant γ-rays can be generated via nonlinear Compton scattering in laser–electron beam interaction.[39–41] In ultrastrong laser fields, the radiation formation length (inversely proportional to the laser intensity) is much smaller than the laser wavelength and cannot carry the driving laser helicity. Thus, the circular polarization of the emitted γ-photons is transferred from the angular momentum (helicity) of electrons[41] (by contrast, the generation of LP γ-photons does not require electron polarization[42]). This mechanism is very different from that in the regimes of Thomson scattering[43,44] and of linear and weakly nonlinear Compton scattering,[45,46] in which the polarization of the emitted γ-photons is transferred from the driving laser field since the radiation formation length is longer than the laser wavelength. Further interaction of the generated polarized high-energy γ-photons with the laser fields could produce electron–positron pairs via the multiphoton Breit–Wheeler process,[47–50] in which case the photon polarization will have a significant effect on the pair production probability.[17,42,47,51–54]

Recently, all-optical γ-photon sources have attracted widespread interest.[55–58] Most of the methods for generating brilliant high-energy γ-rays that have either been experimentally demonstrated or proposed theoretically are based on bremsstrahlung,[59,60] nonlinear Thomson scattering,[57,58] the synchrotron effect,[61,62] betatron oscillations,[63,64] electron wiggling,[65] and nonlinear Compton scattering.[66–69] However, in these innovative works, information about γ-photon polarization has generally been overlooked, in particular, in the regime of strongly nonlinear Compton scattering in the laser–plasma interaction, which actually plays a significant role in subsequent secondary particle generation.[17,42,47,51–54] Therefore, the polarization process of the γ-photons emitted during laser–plasma interaction remains an open question.

In this paper, highly polarized high-energy brilliant γ-rays generated by laser–plasma interaction are studied in the quantum radiation-reaction regime with currently achievable laser intensities.[21–27] We implement electron spin and photon polarization algorithms in two-dimensional (2D) and three-dimensional (3D) particle-in-cell (PIC) EPOCH codes[70,71] in the local constant field approximation[17,49,72–74] to describe spin-resolved electron dynamics semiclassically and photon emission and polarization quantum mechanically.[34,37,38,41,42] We consider a commonly used experimental setup: an ultrastrong LP laser pulse irradiating a near-critical-density (NCD) hydrogen plasma followed by an ultrathin planar aluminum (Al) target (see the interaction scenario in Fig. 1). The electrons in the plasma are first accelerated by the driving laser pulse to ultrarelativistic energies and then collide head-on with the laser pulse reflected by the Al target, emitting abundant LP γ-photons via nonlinear Compton scattering with an average polarization of about 70%, energy up to hundreds of MeV, and brilliance of the order of 10^{21} photons/(s mm^2 mrad^2 0.1%BW) for the given parameters. Compared with laser–electron beam interaction,[41] this scenario is more easily accessible, since only a single laser beam is required. We also show the impact of the laser and target parameters on the γ-ray polarization and brilliance. As a conical gold (Au) target filled with an NCD hydrogen plasma is employed instead of a planar target, for the same driving laser, the collimation and energy of emitted γ-rays are improved, but the polarization rate is reduced, because of the impact of the laser-driven strong quasi-static magnetic field [see the interaction scenario in Fig. 4(a)].

II. SIMULATION METHOD

In this work, we consider laser–plasma interaction in the quantum radiation-reaction regime, which requires a large nonlinear QED parameter $\chi_e \equiv |e|\sqrt{-(F_{\mu\nu}p^\nu)^2}/m^3 \gtrsim 1$.[49,75] Multiphoton Breit–Wheeler pair production is characterized by another nonlinear QED parameter $\chi_\gamma \equiv |e|\sqrt{-(F_{\mu\nu}k_\gamma^\nu)^2}/m^3$.[17,49] Here, p and k_γ are the 4-momenta of the electron and photon, respectively, e and m are the electron charge and mass, respectively, and $F_{\mu\nu}$ is the field tensor. As the electron collides head-on with the laser, one can make the estimate $\chi_e \approx 2a_0\gamma_e\omega_0/m$, with γ_e being the electron Lorentz factor and $a_0 = eE_0/m\omega_0$ the invariant laser field parameter. Here, E_0 and ω_0 are the laser field amplitude and frequency, respectively. Relativistic units with $c = \hbar = 1$ are used throughout.

In our simulation method, we treat spin-resolved electron dynamics semiclassically, and photon emission and pair production quantum mechanically in the local constant field approximation,[17,49,72–74] which is valid at $a_0 \gg 1$. In each simulation step, the photon emission and polarization are both electron-spin-dependent and are calculated using Monte Carlo algorithms[34,41,42] derived in the leading-order approximation with respect to $1/\gamma_e$ via the QED operator method of Baier and Katkov.[76] The photon polarization is represented by the Stokes parameters (ξ_1, ξ_2, ξ_3), defined with respect to the axes $\hat{\mathbf{e}}_1 = \hat{\mathbf{a}} - \hat{\mathbf{v}}\cdot(\hat{\mathbf{v}}\cdot\hat{\mathbf{a}})$ and $\hat{\mathbf{e}}_2 = \hat{\mathbf{v}}\times\hat{\mathbf{a}}$,[77] with the photon emission direction $\hat{\mathbf{n}}$ being along the electron velocity $\mathbf{v}$ for an ultrarelativistic electron (the emission angle $\sim 1/\gamma_e \ll 1$). Here,

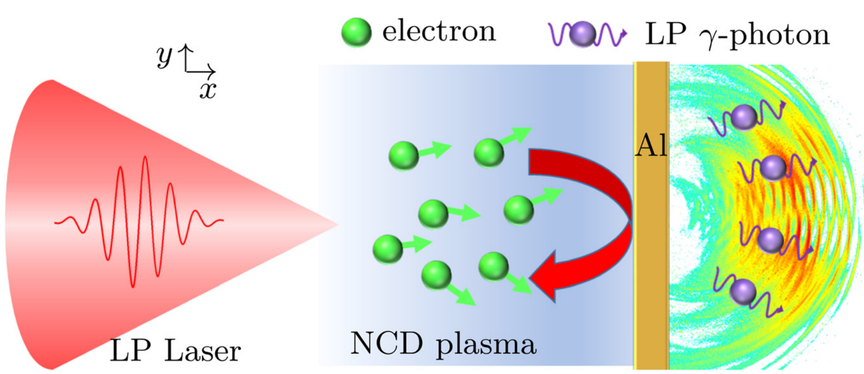

FIG. 1. Scenario for the generation of LP γ-rays via nonlinear Compton scattering. An ultrastrong LP laser pulse, polarized along the y axis and propagating along the x direction, irradiates an NCD hydrogen plasma followed by an ultrathin planar Al target. Laser-driven ultrarelativistic electrons in the plasma collide head-on with the laser pulse reflected by the Al target, emitting LP high-energy γ-photons, which can penetrate through the Al target and propagate forward.

$\hat{\mathbf{v}} = \mathbf{v}/|\mathbf{v}|$, and the unit vector $\hat{\mathbf{a}} = \mathbf{a}/|\mathbf{a}|$ is along the electron acceleration $\mathbf{a}$. On detecting the mean polarization of a γ-photon beam, one must first normalize the Stokes parameters of each photon to the same observation frame $(\hat{\mathbf{o}}_1, \hat{\mathbf{o}}_2, \hat{\mathbf{n}})$, i.e., rotate the Stokes parameters of each photon from its instantaneous frame $(\hat{\mathbf{e}}_1, \hat{\mathbf{e}}_2, \hat{\mathbf{n}})$ to the same observation frame $(\hat{\mathbf{o}}_1, \hat{\mathbf{o}}_2, \hat{\mathbf{n}})$, and then calculate the average Stokes parameters of the γ-photon beam.[41,42,77] Alternatively, in quantum mechanics, the density matrix of photons in terms of the pure state $\mathbf{e}_\alpha$ is given by $\rho_{\alpha\beta} \equiv \mathbf{e}_\alpha \mathbf{e}^*_\beta$, and it can also be expressed as the following combination of the Stokes parameters and the Pauli matrix $\boldsymbol{\sigma}$:[77]

$$\rho_{\alpha\beta} = \frac{1}{2}\begin{pmatrix} 1+\xi_3 & \xi_1 - i\xi_2 \\ \xi_1 + i\xi_2 & 1-\xi_3 \end{pmatrix} = \frac{1}{2}(1 + \xi\cdot\sigma).$$

After photon emission, the electron spin state is determined by the spin-resolved emission probabilities and instantaneously collapses into one of its basis states defined with respect to the instantaneous spin quantization axis (SQA), which is chosen according to the particular observable of interest: to determine the polarization of the electron along the magnetic field in its rest frame, the SQA is chosen along the direction of the magnetic field, $\mathbf{n}_B = \hat{\mathbf{v}} \times \hat{\mathbf{a}}$;[34,37] in the case when the electron beam is initially polarized with initial spin vector $\mathbf{S}_i$, the observable of interest is the spin expectation value along the initial polarization, and the SQA is chosen along that direction.[41] Between photon emissions, the spin precession is governed by the Thomas–Bargmann–Michel–Telegdi equation.[78–80] One can, alternatively, use the Cain code[81] to obtain uniform results.

As emitted high-energy γ-photons interact further with the strong laser fields, electron–positron pairs could be produced by the multiphoton Breit–Wheeler process,[47–50] and the pair production probabilities depend on the photon polarization,[17,47,51–54] which can be calculated using the Monte Carlo method.[42]

III. POLARIZATION OF γ-RAYS GENERATED BY LASER–PLASMA INTERACTION

An ultrastrong LP laser pulse irradiates an NCD hydrogen plasma followed by an ultrathin planar Al target (Fig. 1). Electrons in

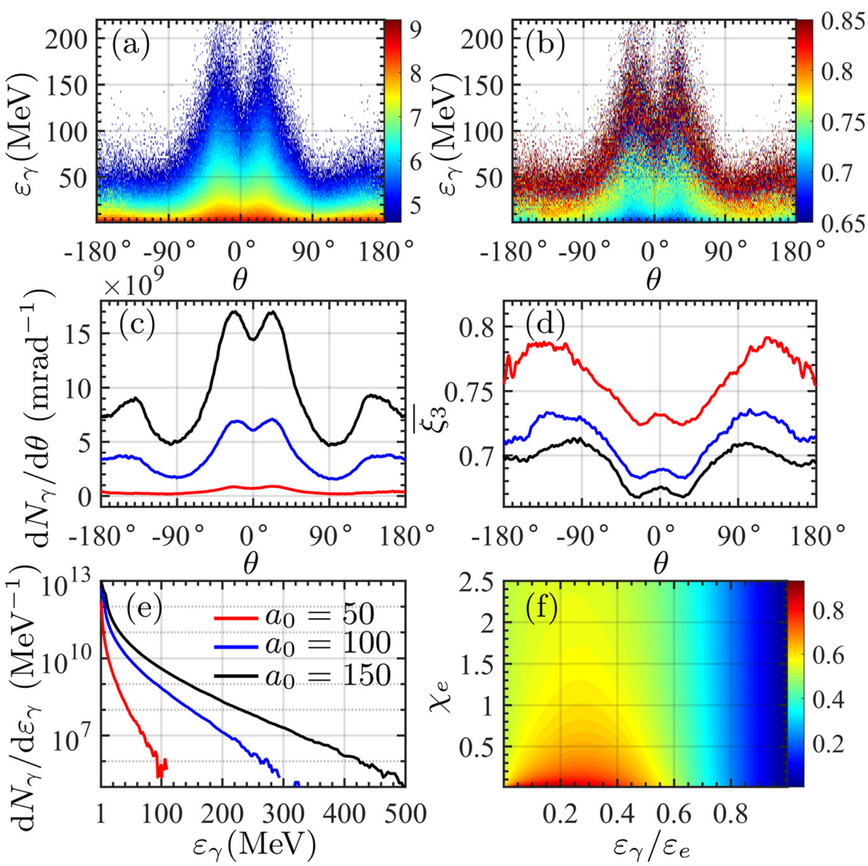

FIG. 2. (a) Angle-resolved density of emitted γ-rays $\log_{10}[d^2N_\gamma/d\varepsilon_\gamma d\theta$ (MeV^{-1} mrad^{-1})] vs γ-photon energy ε_γ and polar angle θ. (b) Linear polarization ξ_3 of emitted γ-photons vs ε_γ and θ. In (a) and (b), $a_0 = 100$. [(c) and (d)] $dN_\gamma/d\theta$ and average linear polarization $\overline{\xi}_3$, respectively, vs θ, calculated by summing over ε_γ in (a) and (b), respectively. (e) $dN_\gamma/d\varepsilon_\gamma$ calculated by summing over θ in (a) vs ε_γ. The red, blue, and black curves in (c)–(e) are for the cases $a_0 = 50$, 100, and 150, respectively. Only γ-photons with $\varepsilon_\gamma \geq 1$ MeV are counted. Other laser and target parameters are given in the text. (f) ξ_3 vs χ_e and $\varepsilon_\gamma/\varepsilon_e$.

the plasma are accelerated to ultrarelativistic energies and then collide head-on with the laser pulse reflected by the Al target, emitting abundant LP high-energy γ-photons. To maximize the reflection of the driving laser pulse, the thickness of the Al target should be greater than the laser piston depth.[82] In fact, as the emitted γ-photons penetrate through the Al target, an appropriate thickness can also mitigate bremsstrahlung and Bethe-Heitler pair production, which usually requires a thickness of the order of millimeters.[83,84]

The simulation box employed is $x \times y = 40\lambda_0 \times 30s\lambda_0$, and the corresponding cells are 1000×750. An LP laser pulse injected from the left boundary polarizes along the y axis and propagates along the x direction with wavelength $\lambda_0 = 1$ μm and normalized intensity $a = a_0 \exp[-(t-t_0)^2/\tau^2]\exp(-y^2/w_0^2)$, where the focal radius $w_0 = 5\lambda_0$ and the pulse duration $\tau = 9T_0$, with laser period T_0, corresponding to a full width at half maximum (FWHM) $\tau' = 2\sqrt{\ln 2}\,\tau \approx 15T_0$, and a time delay $t_0 = \tau$ is adopted. A solid planar Al target with electron density $n_e^{\mathrm{Al}} = 702n_c$ and thickness $d_{\mathrm{Al}} = 1$ μm is placed 20 μm from the right boundary, where the plasma critical density $n_c = m\omega_0^2/4\pi e^2 \approx 1.1 \times 10^{21}$ cm^{-3}. The left side of the Al target is filled with an NCD hydrogen plasma with electron density $n_e = 5n_c$ and thickness $d_p = 10$ μm. The numbers of macroparticles in each cell are 100 for electrons and 20 for H^+ and for Al^{13+} (fully ionized).

Distributions of the density and linear polarization of emitted γ-rays are illustrated in Figs. 2(a) and 2(b), respectively, with the laser peak intensity $I_0 \approx 1.38 \times 10^{22}$ W/cm^2 ($a_0 = 100$).[21–27] High-energy γ-photons with $\epsilon_\gamma \gtrsim 100$ MeV are mainly emitted forward, and two density peaks arise near $\theta \approx \pm 21^\circ$, since the γ-photons are assumed to be emitted along the electron momentum, and the electron propagation angle $\theta_e \propto p_e^\perp/p_e^\parallel \propto a_R/\gamma_e$ (the electrons interact with the reflected laser pulse with invariant intensity parameter a_R and $a_R \propto \overline{a} \propto a_0$ with an average laser intensity $\overline{a}$), as shown in Fig. 2(a), which is in excellent agreement with other simulations.[85] The linear polarization of γ-photons is characterized by the Stokes parameters ξ_1 and ξ_3.[41,42,77] As we employ the basis vector of the observation frame $\hat{\mathbf{o}}_1$ in the polarization y–x plane of the driving laser, and because γ-photons are emitted mainly in the polarization plane, ξ_1 is negligible and ξ_3 is as given in Fig. 2(b): at a given polar angle, the linear polarization ξ_3 for higher-energy γ-photons is larger. The average linear polarization $\overline{\xi_3} \approx 0.68$, and the partial ξ_3 can reach up to 0.73. In nonlinear Compton scattering, the circular polarization defined by ξ_2 requires initially longitudinally spin-polarized electrons[41] and is negligible here.

To make the results in Figs. 2(a) and 2(b) clearer, we sum over ε_γ to obtain the angle-resolved number and linear polarization of emitted γ-photons shown by the blue curves in Figs. 2(c) and 2(d), and we sum over θ in Fig. 2(a) to obtain the energy density shown by the blue curve in Fig. 2(e). The impact of the driving laser intensity a_0 can be seen from Figs. 2(c)–2(e). In ultrastrong laser fields, in one laser period T_0, the number of formation lengths (in which a photon could be emitted) is proportional to the invariant laser intensity, and the photon emission probability in each formation length is proportional to the fine structure constant α,[28,49] and thus the number of emitted γ-photons $N_\gamma \propto N_e' \alpha a_R \tau/T_0 \propto a_0$, where N_e' is the number of parental electrons and is proportional to the target density n_e and laser focal spot size w_0: $N_e' \propto n_e \pi w_0^2$. Since $a_0 \gg 1$, nearly all atoms within the focal spot can be fully ionized. As a_0 increases from 50 to 150, N_γ also continuously increases, the reflected laser intensity a_R and the electron energy γ_e are both increased, and consequently the peak angle $\theta \propto a_R/\gamma_e$ increases slightly [Fig. 2(c)]. $\varepsilon_\gamma \propto \varepsilon_e \chi_e$, where the electron energy $\varepsilon_e \sim a_0$ (i.e., a stronger driving laser can accelerate electrons to

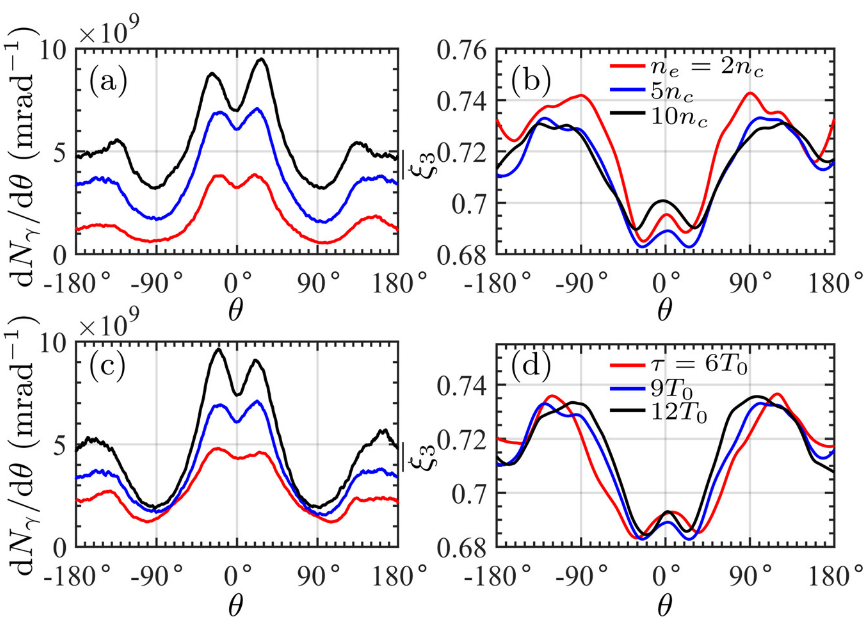

FIG. 3. (a) and (b) $dN_\gamma/d\theta$ and $\overline{\xi_3}$, respectively, vs θ for the cases $n_e = 2n_c$ (red), $5n_c$ (blue), and $10n_c$ (black). [(c) and (d)] $dN_\gamma/d\theta$ and $\overline{\xi_3}$, respectively, vs θ for the cases $\tau = 6T_0$ (red), $9T_0$ (blue), and $12T_0$ (black). $a_0 = 100$, and other laser and target parameters are the same as those in Fig. 2.

higher energies) and $\chi_e \propto a_R\gamma_e \propto a_0\varepsilon_e$, and thus, as a_0 increases, ε_γ increases as well [Fig. 2(e)].

We underline that $\overline{\xi_3}$ decreases monotonically with increasing a_0, as shown in Fig. 2(d). The physical reason for this is as follows. The Stokes parameter ξ_3 depends sensitively on the parameters χ_e and $\varepsilon_\gamma/\varepsilon_e$ (see the analytical expression for ξ_3 in Refs. 41 and 42), as demonstrated in Fig. 2(f). As χ_e increases in the region under consideration, ξ_3 decreases continuously; as $\varepsilon_\gamma/\varepsilon_e$ increases, ξ_3 first increases slightly and then gradually decreases to 0. Consequently, as $\chi_e \propto a_0$ increases, $\overline{\xi_3}$ decreases in Fig. 2(d); i.e., lower-intensity driving laser pulses can generate higher-polarization (but lower-brilliance) γ-photons.

In the case $a_0 = 100$, the radius and duration of the emitted γ-ray beam are $w_\gamma \approx w_0$ and $\tau_\gamma \approx \tau'$, respectively. The angular divergences (FWHM) are approximately 1.74×1.74 rad^2, 1.47×1.47 rad^2, 1.39×1.39 rad^2, and 1.36×1.36 rad^2 for $\varepsilon_\gamma \geq 1$ MeV, 10 MeV, 100 MeV, and 200 MeV, respectively. The corresponding brilliances are 0.67×10^{21}, 2×10^{19}, 7×10^{18}, and 2×10^{17} photons/(s mm^2 mrad^2 0.1% BW) for $\varepsilon_\gamma = 1$ MeV, 10 MeV, 100 MeV, and 200 MeV, respectively. It is obvious that the brilliance $\propto N_r \propto a_0$. For the given parameters, the multiphoton Breit–Wheeler pair production probabilities during the interactions of γ-photons with the laser fields are rather low, since $\chi_\gamma \ll 1$.

Note that for the given parameters, as the γ-photons propagate through the plasma, the photon polarization flips (depolarization) in the background fields (vacuum polarization), and the collisions with the plasma particles (involving Compton scattering and Bethe–Heitler pair production) are estimated to be negligible.[17,86]

With the aim of determining experimental feasibility, the impact of laser and plasma parameters on the density and polarization degree of emitted γ-photons is shown in Fig. 3. For instance, as the plasma density n_e or the driving laser pulse duration τ increases, $N_\gamma \propto N_e'\alpha a_R\tau/T_0 \propto n_e\tau$ also increases [Figs. 3(a) and 3(c)]. However, for an NCD plasma, $\overline{\xi_3}$ changes only slightly with variations in n_e and τ [Figs. 3(b) and 3(d)]. Note that as n_e increases from $2n_c$ to $10n_c$, the

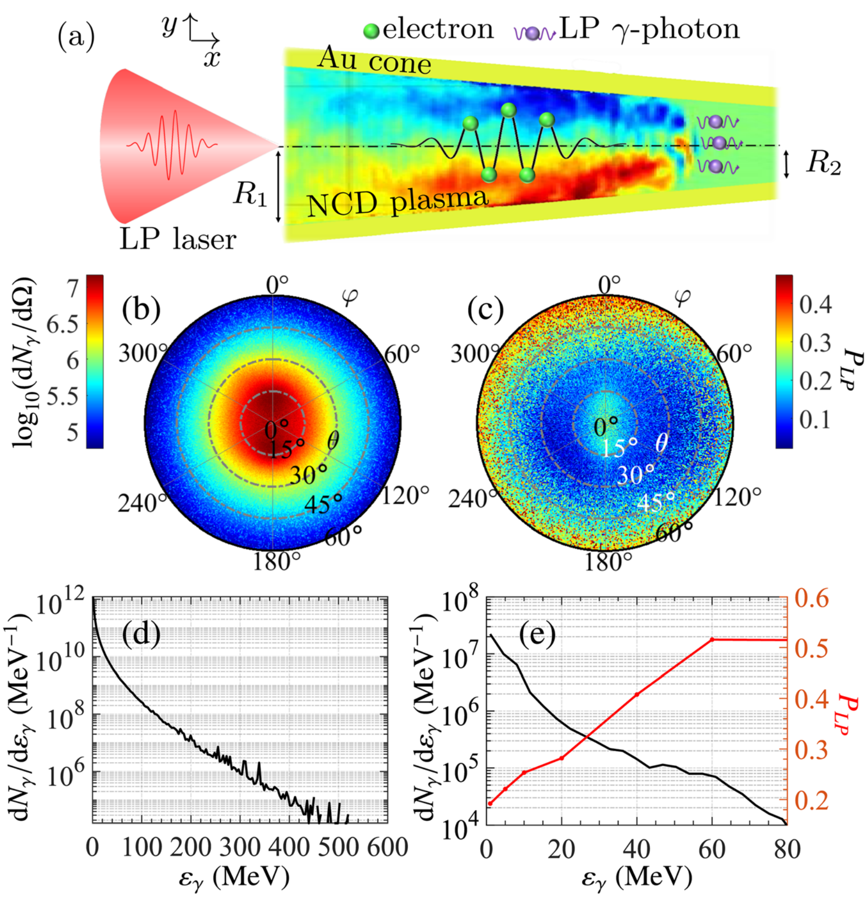

FIG. 4. (a) Scenario for the generation of LP γ-rays by an ultrastrong LP laser pulse, polarizing along the y axis and propagating along the x direction, interacting with a conical Au target filled with an NCD hydrogen plasma. The red and blue areas inside the cone indicate the quasi-static magnetic fields along the $+z$ and $-z$ directions, respectively, caused by the driving laser pulse. (b) Plot of $\log_{10}(dN_\gamma/d\Omega)$ with respect to the polar angle θ and the azimuthal angle ϕ, where the solid angle $d\Omega = \sin\theta\, d\theta\, d\phi$. (c) Plot of the linear polarization P_{LP} with respect to θ and ϕ, where $P_{LP} = \sqrt{\xi_1^2 + \xi_3^2}$. (d) Total energy spectra of emitted γ-photons $dN_\gamma/d\varepsilon_\gamma$ vs ε_γ. (e) $dN_\gamma/d\varepsilon_\gamma$ (black) and P_{LP} (red) vs ε_γ at angles $(\theta, \phi) = (10^\circ \pm 0.3^\circ, 180^\circ \pm 0.3^\circ)$, where P_{LP} is the average linear polarization of γ-photons with energies $\geq \varepsilon_\gamma$. The results in (b)–(e) are calculated with $\varepsilon_\gamma \geq 1$ MeV at $t = 110T_0$, when the interaction has finished. The laser parameters are the same as those in Figs. 2(a) and 2(b), and the target parameters are given in the text.

opacity of the plasma increases as well, and laser propagation becomes more and more unstable, which results in an asymmetric angular distribution of emitted γ-rays,[61] as shown in Fig. 3(a). Meanwhile, in the plasma, as a result of the driving laser pulse pushing the electrons in the low-density region forward, a high-density region can be created, where unstable laser propagation further induces asymmetric γ-photon emission. This effect becomes more severe as the laser pulse duration τ increases, as shown in Fig. 3(c). As already shown in Fig. 2, the peak angle of the γ-ray spectrum $\theta \propto a_R/\gamma_e$, and a_R and γ_e here both depend on the laser and plasma parameters (e.g., a_0, τ, and n_e). It is difficult to obtain analytical relations between θ and these parameters; however, our simulation results in Figs. 2(c), 3(a), and 3(c) indicate that the peak angle θ changes only slightly when these parameters vary, which is advantageous for experimental observations.

Furthermore, instead of the planar target in Figs. 1 and 2, we now consider a conical Au target filled with an NCD hydrogen plasma [Fig. 4(a)]. The front and rear surfaces of the cone are open. As an ultraintense LP laser pulse irradiates the NCD hydrogen plasma inside the Au cone, almost all the bulk electrons are pushed forward and excite a strong quasi-static magnetic field B_p.[61,66] The maximum intensity of the magnetic field can be estimated as $\max(B_p) \simeq 4\pi|e|\beta_e n_e R$, which is of the same order of magnitude as the magnetic field of the driving laser.[61] Here, R and β_e denote the radius of the cone and the electron velocity scaled by the light speed in vacuum. For the plane-wave case, the transverse electric field $\mathbf{E}_\perp$ can almost cancel $\mathbf{v}\cdot\mathbf{B}$ with the magnetic field $\mathbf{B}$, and consequently χ_e is rather small and the photon emission is very weak. However, in the case of a conical target with a strong quasi-static magnetic field B_p, $\chi_e \propto B_p$ greatly increases, and thus subsequent γ-photon emission is significantly enhanced. Furthermore, since most photons are emitted at the edge of the cone, where the transverse velocities of electrons are close to 0, the angular spread of the γ-ray beam is narrowed.[61]

In Fig. 4, the simulation box is $x \times y \times z = 110\lambda_0 \times 40\lambda_0 \times 40\lambda_0$, and the corresponding cells are $2200 \times 400 \times 400$. A solid conical Au target with electron density $n_e^{\mathrm{Au}} = 100n_c$ and thickness $d_{\mathrm{Au}} = 1\ \mu$m is located in the region from $5\lambda_0$ to $75\lambda_0$ on the x axis. The left and right opening radii of the cone are $R_1 = 7\lambda_0$ and $R_2 = 3\lambda_0$, respectively. The Au cone is filled with an NCD hydrogen plasma of density $n_e = 5n_c$. The numbers of macroparticles in each cell are 100 for electrons and 20 for H^+ and for Au^{2+} (partially ionized). The angle-resolved density of emitted γ-photons is illustrated in Fig. 4(b). Compared with the case of a planar target employing the same driving laser, the collimation and cutoff energy of the emitted γ-photons in the case of a conical target are much better, since the conical target has a greater longitudinal size and generates strong confinement effects derived from the transverse magnetic field. For instance, most γ-photons concentrate in the angular region $\theta \lesssim 20^\circ$, and the cutoff energy exceeds 450 MeV, as shown in Fig. 4(d); see for comparison the corresponding values for a planar target in Fig. 2. The azimuthal magnetic field generated in the conical target results in a transverse (azimuthal) spread of the electron dynamics and further γ-photon emission. This reduces the average polarization rate of the γ-rays, as shown in Fig. 4(c), because γ-photons polarized along different azimuthal angles cancel each other in the average polarization. For instance, the energy density and polarization of the γ-photons at a specific solid angle $(\theta, \phi) = (10^\circ \pm 0.3^\circ, 180^\circ \pm 0.3^\circ)$ near the γ-ray beam center are illustrated in Fig. 4(e). The linear polarization and the energy density are respectively proportional and inversely proportional to the γ-photon energy. For $\varepsilon_\gamma \geq 20$ MeV, 40 MeV, and 60 MeV, the linear polarizations $P_{\mathrm{LP}} \approx 0.28$, 0.41, and 0.52, respectively, and the brilliances are approximately 0.86×10^{20}, 0.43×10^{20}, and 0.30×10^{20} photons/(s mm^2 mrad^2 0.1% BW), respectively.

IV. CONCLUSION

Generation of highly polarized high-energy brilliant γ-rays has been studied through investigating the interaction of a single-shot ultraintense LP laser pulse with a solid target filled with an NCD plasma in the quantum radiation-reaction regime. The results show that with currently achievable laser intensities, the emitted γ-rays could reach an average linear polarization of about 70%, an energy up to hundreds of MeV, and a brilliance of the order of 10^{21} photons/(s mm^2 mrad^2 0.1% BW), and could have applications in high-energy physics and laboratory astrophysics.

AUTHORS' CONTRIBUTIONS

K.X. and Z.-K.D. contributed equally to this work.

ACKNOWLEDGMENTS

This work is supported by the National Natural Science Foundation of China (Grant Nos. 11874295, 11875219, 11705141, 11905169, and 11875319), the National Key R&D Program of China (Grant Nos. 2018YFA0404801 and 2018YFA0404802), Chinese Science Challenge Project No. TZ2016005, and National Key Research and Development Project No. 2019YFA0404900.

REFERENCES

[1] U. I. Uggerhøj, "The interaction of relativistic particles with strong crystalline fields," Rev. Mod. Phys. **77**, 1131–1171 (2005).

[2] G. Moortgat-Pick, T. Abe, G. Alexander *et al.*, "Polarized positrons and electrons at the linear collider," Phys. Rep. **460**, 131–243 (2008).

[3] C. Bœhm, C. Degrande, O. Mattelaer, and A. C. Vincent, "Circular polarisation: A new probe of dark matter and neutrinos in the sky," J. Cosmol. Astropart. Phys. **2017**, 043.

[4] P. Laurent, J. Rodriguez, J. Wilms, M. Cadolle Bel, K. Pottschmidt, and V. Grinberg, "Polarized gamma-ray emission from the galactic black hole cygnus X-1," Science **332**, 438–439 (2011).

[5] J. Speth and A. van der Woude, "Giant resonances in nuclei," Rep. Prog. Phys. **44**, 719–786 (1981).

[6] Z. Akbar, P. Roy, S. Park *et al.*, "Measurement of the helicity asymmetry e in $\omega \to \pi^+\pi^-\pi^0$ photoproduction," Phys. Rev. C **96**, 065209 (2017).

[7] B. King and N. Elkina, "Vacuum birefringence in high-energy laser-electron collisions," Phys. Rev. A **94**, 062102 (2016).

[8] A. Ilderton and M. Marklund, "Prospects for studying vacuum polarisation using dipole and synchrotron radiation," J. Plasma Phys. **82**, 655820201 (2016).

[9] S. Ataman, M. Cuciuc, L. D'Alessi, L. Neagu, M. Rosu, K. Seto, O. Tesileanu, Y. Xu, and M. Zeng, "Experiments with combined laser and gamma beams at ELI-NP," AIP Conf. Proc. **1852**, 070002 (2017).

[10] Y. Nakamiya and K. Homma, "Probing vacuum birefringence under a high-intensity laser field with gamma-ray polarimetry at the GeV scale," Phys. Rev. D **96**, 053002 (2017).

[11] S. Bragin, S. Meuren, C. H. Keitel, and A. Di Piazza, "High-energy vacuum birefringence and dichroism in an ultrastrong laser field," Phys. Rev. Lett. **119**, 250403 (2017).

[12] H. Olsen and L. C. Maximon, "Photon and electron polarization in high-energy bremsstrahlung and pair production with screening," Phys. Rev. **114**, 887–904 (1959).

[13]D. Abbott *et al.* (PEPPo Collaboration), "Production of highly polarized positrons using polarized electrons at MeV energies," Phys. Rev. Lett. **116**, 214801 (2016).
[14]T. Omori, M. Fukuda, T. Hirose *et al.*, "Efficient propagation of polarization from laser photons to positrons through Compton scattering and electron-positron pair creation," Phys. Rev. Lett. **96**, 114801 (2006).
[15]G. Alexander, J. Barley, Y. Batygin *et al.*, "Observation of polarized positrons from an undulator-based source," Phys. Rev. Lett. **100**, 210801 (2008).
[16]V. Petrillo, A. Bacci, C. Curatolo *et al.*, "Polarization of x-gamma radiation produced by a Thomson and Compton inverse scattering," Phys. Rev. Spec. Top.–Accel. Beams **18**, 110701 (2015).
[17]V. N. Baier, V. M. Katkov, and V. M. Strakhovenko, *Electromagnetic Processes at High Energies in Oriented Single Crystals* (World Scientific, Singapore, 1998).
[18]D. Lohmann, J. Peise, J. Ahrens *et al.*, "Linearly polarized photons at MAMI (Mainz)," Nucl. Instrum. Methods Phys. Res., Sect. A **343**, 494–507 (1994).
[19]R. Carrigan and J. Ellison, *Relativistic Channeling* (Plenum, New York, 1987).
[20]V. M. Biryukov, Y. A. Chesnokov, and V. I. Kotov, *Crystal Channeling and its Application at High Energy Accelerators* (Springer, Berlin, 1997).
[21]J. W. Yoon, C. Jeon, J. Shin, S. K. Lee, H. W. Lee, I. W. Choi, H. T. Kim, J. H. Sung, and C. H. Nam, "Achieving the laser intensity of 5.5×10^{22} W/cm^2 with a wavefront-corrected multi-PW laser," Opt. Express **27**, 20412–20420 (2019).
[22]C. N. Danson, C. Haefner, J. Bromage *et al.*, "Petawatt and exsawatt class lasers worldwide," High Power Laser Sci. Eng. **7**, e54 (2019).
[23]S. Gales, K. A. Tanaka, D. L. Balabanski *et al.*, "The extreme light infrastructure–nuclear physics (ELI-NP) facility: New horizons in physics with 10 PW ultra-intense lasers and 20 MeV brilliant gamma beams," Rep. Prog. Phys. **81**, 094301 (2018).
[24]See http://www.eli-beams.eu/en/facility/lasers/ for The Extreme Light Infrastructure (ELI).
[25]See http://www.clf.stfc.ac.uk/Pages/The-Vulcan-10-Petawatt-Project.aspx for The Vulcan Facility.
[26]See http://www.xcels.iapras.ru/ for Exawatt Center for Extreme Light Studies (XCELS).
[27]See https://www.ibs.re.kr/eng/sub02_03_05.do for T. C. for Relativistic Laser Science (CoReLS).
[28]A. Negoita, C. Müller, K. Z. Hatsagortsyan, and C. H. Keitel, "Extremely high-intensity laser interactions with fundamental quantum systems," Rev. Mod. Phys. **84**, 1177–1228 (2012).
[29]T. G. Blackburn, "Radiation reaction in electron-beam interactions with high-intensity lasers," Rev. Mod. Plasma Phys. **4**, 5 (2020).
[30]D. Del Sorbo, D. Seipt, T. G. Blackburn, A. G. R. Thomas, C. D. Murphy, J. G. Kirk, and C. P. Ridgers, "Spin polarization of electrons by ultraintense lasers," Phys. Rev. A **96**, 043407 (2017).
[31]D. Del Sorbo, D. Seipt, A. G. R. Thomas, and C. P. Ridgers, "Electron spin polarization in realistic trajectories around the magnetic node of two counter-propagating, circularly polarized, ultra-intense lasers," Plasma Phys. Controlled Fusion **60**, 064003 (2018).
[32]D. Seipt, D. Del Sorbo, C. P. Ridgers, and A. G. R. Thomas, "Theory of radiative electron polarization in strong laser fields," Phys. Rev. A **98**, 023417 (2018).
[33]D. Seipt, D. Del Sorbo, C. P. Ridgers, and A. G. R. Thomas, "Ultrafast polarization of an electron beam in an intense bichromatic laser field," Phys. Rev. A **100**, 061402(R) (2019).
[34]Y.-F. Li, R. Shaisultanov, K. Z. Hatsagortsyan, F. Wan, C. H. Keitel, and J.-X. Li, "Ultrarelativistic electron-beam polarization in single-shot interaction with an ultraintense laser pulse," Phys. Rev. Lett. **122**, 154801 (2019).
[35]H.-H. Song, W.-M. Wang, J.-X. Li, Y.-F. Li, and Y.-T. Li, "Spin-polarization effects of an ultrarelativistic electron beam in an ultraintense two-color laser pulse," Phys. Rev. A **100**, 033407 (2019).
[36]Y.-F. Li, R.-T. Guo, R. Shaisultanov, K. Z. Hatsagortsyan, and J.-X. Li, "Electron polarimetry with nonlinear Compton scattering," Phys. Rev. Appl. **12**, 014047 (2019).
[37]Y.-Y. Chen, P.-L. He, R. Shaisultanov, K. Z. Hatsagortsyan, and C. H. Keitel, "Polarized positron beams via intense two-color laser pulses," Phys. Rev. Lett. **123**, 174801 (2019).
[38]F. Wan, R. Shaisultanov, Y.-F. Li, K. Z. Hatsagortsyan, C. H. Keitel, and J.-X. Li, "Ultrarelativistic polarized positron jets via collision of electron and ultraintense laser beams," Phys. Lett. B **800**, 135120 (2020).
[39]D. Y. Ivanov, G. L. Kotkin, and V. G. Serbo, "Complete description of polarization effects in emission of a photon by an electron in the field of a strong laser wave," Eur. Phys. J. C **36**, 127–145 (2004).
[40]B. King, N. Elkina, and H. Ruhl, "Photon polarization in electron-seeded pair-creation cascades," Phys. Rev. A **87**, 042117 (2013).
[41]Y.-F. Li, R. Shaisultanov, Y.-Y. Chen, F. Wan, K. Z. Hatsagortsyan, C. H. Keitel, and J.-X. Li, "Polarized ultrashort brilliant multi-GeV γ rays via single-shot laser-electron interaction," Phys. Rev. Lett. **124**, 014801 (2020).
[42]F. Wan, Y. Wang, R.-T. Guo, Y.-Y. Chen, R. Shaisultanov, Z.-F. Xu, K. Z. Hatsagortsyan, C. H. Keitel, and J.-X. Li, "High-energy γ-photon polarization in nonlinear Breit-Wheeler pair production and γ-polarimetry," arXiv:2002.10346.
[43]K. Kawase, M. Kando, T. Hayakawa *et al.*, "Sub-MeV tunably polarized X-ray production with laser Thomson backscattering," Rev. Sci. Instrum. **79**, 053302 (2008).
[44]G.-P. An, Y.-L. Chi, Y.-L. Dang *et al.*, "High energy and high brightness laser Compton backscattering gamma-ray source at IHEP," Matter Radiat. Extremes **3**, 219–226 (2018).
[45]B. Fu and S. Tang, "Nonlinear Compton scattering of polarised photons in plane-wave backgrounds," arXiv:2003.01749 (2020).
[46]S. Tang, B. King, and H. Hu, "Highly polarised gamma photons from electron-laser collisions," arXiv:2003.03246 (2020).
[47]G. Breit and J. A. Wheeler, "Collision of two light quanta," Phys. Rev. **46**, 1087–1091 (1934).
[48]H. R. Reiss, "Absorption of light by light," J. Math. Phys. **3**, 59–67 (1962).
[49]V. I. Ritus, "Quantum effects of the interaction of elementary particles with an intense electromagnetic field," J. Sov. Laser Res. **6**, 497 (1985).
[50]C. Bula, K. T. McDonald, E. J. Prebys *et al.*, "Observation of nonlinear effects in Compton scattering," Phys. Rev. Lett. **76**, 3116–3119 (1996).
[51]L. S. Brown and T. W. B. Kibble, "Interaction of intense laser beams with electrons," Phys. Rev. **133**, A705–A719 (1964).
[52]A. I. Nikishov and V. I. Ritus, "Quantum processes in the field of a plane electromagnetic wave and in a constant field," Sov. Phys. JETP **19**, 529 (1964) [Zh. Eksp. Teor. Fiz. **46**, 776 (1964)].
[53]J. W. Motz, H. A. Olsen, and H. W. Koch, "Pair production by photons," Rev. Mod. Phys. **41**, 581–639 (1969).
[54]D. Y. Ivanov, G. L. Kotkin, and V. G. Serbo, "Complete description of polarization effects in e^+e^- pair production by a photon in the field of a strong laser wave," Eur. Phys. J. C **40**, 27 (2005).
[55]K. T. Phuoc, S. Corde, C. Thaury, V. Malka, A. Tafzi, J. P. Goddet, R. C. Shah, S. Sebban, and A. Rousse, "All-optical Compton gamma-ray source," Nat. Photonics **6**, 308 (2012).
[56]S. Chen, N. D. Powers, I. Ghebregziabher *et al.*, "MeV-energy x rays from inverse Compton scattering with laser-wakefield accelerated electrons," Phys. Rev. Lett. **110**, 155003 (2013).
[57]G. Sarri, D. J. Corvan, W. Schumaker *et al.*, "Ultrahigh brilliance multi-MeV γ-ray beams from nonlinear relativistic Thomson scattering," Phys. Rev. Lett. **113**, 224801 (2014).
[58]W. Yan, C. Fruhling, G. Golovin, D. Haden, J. Luo, P. Zhang, B. Zhao, J. Zhang, C. Liu, M. Chen, S. Chen, S. Banerjee, and D. Umstadter, "High-order multiphoton Thomson scattering," Nat. Photonics **11**, 514–520 (2017).
[59]Y. Glinec, J. Faure, L. L. Dain, S. Darbon, T. Hosokai, J. J. Santos, E. Lefebvre, J. P. Rousseau, F. Burgy, B. Mercier, and V. Malka, "High-resolution γ-ray radiography produced by a laser-plasma driven electron source," Phys. Rev. Lett. **94**, 025003 (2005).
[60]A. Giulietti, N. Bourgeois, T. Ceccotti *et al.*, "Intense γ-ray source in the giant-dipole-resonance range driven by 10-TW laser pulses," Phys. Rev. Lett. **101**, 105002 (2008).

[61] D. J. Stark, T. Toncian, and A. V. Arefiev, "Enhanced multi-MeV photon emission by a laser-driven electron beam in a self-generated magnetic field," Phys. Rev. Lett. **116**, 185003 (2016).

[62] A. Benedetti, M. Tamburini, and C. H. Keitel, "Giant collimated gamma-ray flashes," Nat. Photonics **12**, 319 (2018).

[63] H. X. Chang, B. Qiao, T. W. Huang, Z. Xu, C. T. Zhou, Y. Q. Gu, X. Q. Yan, M. Zepf, and X. T. He, "Brilliant petawatt gamma-ray pulse generation in quantum electrodynamic laser-plasma interaction," Sci. Rep. **7**, 45031 (2017).

[64] T.-P. Yu, A. Pukhov, Z.-M. Sheng, F. Liu, and G. Shvets, "Bright betatronlike x rays from radiation pressure acceleration of a mass-limited foil target," Phys. Rev. Lett. **110**, 045001 (2013).

[65] W.-M. Wang, Z.-M. Sheng, P. Gibbon, L.-M. Chen, Y.-T. Li, and J. Zhang, "Collimated ultrabright gamma rays from electron wiggling along a petawatt laser-irradiated wire in the QED regime," Proc. Natl. Acad. Sci. U. S. A. **115**, 9911 (2018).

[66] X.-L. Zhu, Y. Yin, T.-P. Yu, F.-Q. Shao, Z.-Y. Ge, W.-Q. Wang, and J.-J. Liu, "Enhanced electron trapping and γ-ray emission by ultra-intense laser irradiating a near-critical-density plasma filled gold cone," New J. Phys. **17**, 053039 (2015).

[67] X.-L. Zhu, M. Chen, T.-P. Yu, S.-M. Weng, L.-X. Hu, P. McKenna, and Z.-M. Sheng, "Bright attosecond γ-ray pulses from nonlinear Compton scattering with laser-illuminated compound targets," Appl. Phys. Lett. **112**, 174102 (2018).

[68] Y.-J. Gu, O. Klimo, S. V. Bulanov, and S. Weber, "Brilliant gamma-ray beam and electron-positron pair production by enhanced attosecond pulses," Commun. Phys. **1**, 93 (2018).

[69] Y.-J. Gu, M. Jirka, O. Klimo, and S. Weber, "Gamma photons and electron-positron pairs from ultra-intense laser-matter interaction: A comparative study of proposed configurations," Matter Radiat. Extremes **4**, 064403 (2019).

[70] C. P. Ridgers, C. S. Brady, R. Duclous, J. G. Kirk, K. Bennett, T. D. Arber, A. P. L. Robinson, and A. R. Bell, "Dense electron-positron plasmas and ultraintense γ rays from laser-irradiated solids," Phys. Rev. Lett. **108**, 165006 (2012).

[71] T. D. Arber, K. Bennett, C. S. Brady *et al.*, "Contemporary particle-in-cell approach to laser-plasma modelling," Plasma Phys. Controlled Fusion **57**, 113001 (2015).

[72] A. Di Piazza, M. Tamburini, S. Meuren, and C. H. Keitel, "Implementing nonlinear Compton scattering beyond the local-constant-field approximation," Phys. Rev. A **98**, 012134 (2018).

[73] A. Ilderton, "Note on the conjectured breakdown of QED perturbation theory in strong fields," Phys. Rev. D **99**, 085002 (2019).

[74] A. Di Piazza, M. Tamburini, S. Meuren, and C. H. Keitel, "Improved local-constant-field approximation for strong-field QED codes," Phys. Rev. A **99**, 022125 (2019).

[75] J. Koga, T. Z. Esirkepov, and S. V. Bulanov, "Nonlinear Thomson scattering in the strong radiation damping regime," Phys. Plasmas **12**, 093106 (2005).

[76] V. N. Baier, V. M. Katkov, and V. S. Fadin, *Radiation from Relativistic Electrons* (Atomizdat, Moscow, 1973).

[77] W. H. McMaster, "Matrix representation of polarization," Rev. Mod. Phys. **33**, 8–28 (1961).

[78] L. H. Thomas, "The motion of the spinning electron," Nature **117**, 514 (1926).

[79] L. H. Thomas, "The kinematics of an electron with an axis," Philos. Mag. **3**, 1–22 (1927).

[80] V. Bargmann, L. Michel, and V. L. Telegdi, "Precession of the polarization of particles moving in a homogeneous electromagnetic field," Phys. Rev. Lett. **2**, 435–436 (1959).

[81] K. Yokoya, CAIN2.42 Users Manual, https://ilc.kek.jp/~yokoya/CAIN/Cain242/.

[82] A. P. L. Robinson, P. Gibbon, M. Zepf, S. Kar, R. G. Evans, and C. Bellei, "Relativistically correct hole-boring and ion acceleration by circularly polarized laser pulses," Plasma Phys. Controlled Fusion **51**, 024004 (2009).

[83] T. Erber, "High-energy electromagnetic conversion processes in intense magnetic fields," Rev. Mod. Phys. **38**, 626–659 (1966).

[84] O. J. Pike, F. Mackenroth, E. G. Hill, and S. J. Rose, "A photon–photon collider in a vacuum hohlraum," Nat. Photonics **8**, 434–436 (2014).

[85] Y. Lu, H. Zhang, Y.-T. Hu, J. Zhao, L.-X. Hu, D.-B. Zou, X.-R. Xu, W.-Q. Wang, K. Liu, and T.-P. Yu, "Effect of laser polarization on the electron dynamics and photon emission in near-critical-density plasmas," Plasma Phys. Controlled Fusion **62**, 035002 (2020).

[86] V. B. Berestetskii, E. M. Lifshitz, and L. P. Pitaevskii, *Quantum Electrodynamics* (Pergamon, Oxford, 1982).